SPE 66537

Numerical Modeling of Aquifer Disposal of CO2

Karsten Pruess, SPE, Tianfu Xu, John Apps and Julio Garcia, Lawrence Berkeley National Laboratory

This paper was prepared for presentation at the SPE/EPA/DOE Exploration and Production Environmental Conference held in San Antonio, Texas, 26—28 February 2001.

Abstract

Disposal of CO2 from stationary sources (fossil-fired power plants) into brackish (saline) aquifers has been suggested as a possible means for reducing emissions of greenhouse gases into the atmosphere. Injection of CO2 into such aquifers would be carried out at supercritical conditions, and would give rise to the evolution of a two-phase fluid system, in which most of the injected CO2 will reside in a dense supercritical gas phase, while also dissolving partially into the aqueous phase, and reacting with native minerals. This paper presents scoping studies of the amounts of CO2 that can be trapped into the various phases (gas, aqueous, and solid) for a range of conditions that may be encountered in typical disposal aquifers. Our analyses employ a realistic fluid property (PVT) description of brine-CO2 mixtures for super-critical conditions, which takes into account real gas density and viscosity effects for CO2, and includes pressure, temperature, and salinity dependence of CO2 dissolution into the aqueous phase. The fluid property description has been incorporated into a multi-purpose reservoir simulator, and has been used to evaluate dynamic effects of CO2 injection into aquifers. A survey of minerals commonly encountered in crustal rocks was made to identify possibilities for chemical sequestration of CO2 through the formation of carbonates of low solubility. We also performed batch reaction modeling of the geochemical evolution of representative aquifer mineralogies. Results indicate that under favorable conditions the amount of CO2 that may be sequestered by precipitation of secondary carbonates is comparable to the amount of CO2 dissolved in pore waters. The accumulation of carbonates in the rock matrix and induced rock mineral alteration due to the presence of dissolved CO2 lead to a considerable decrease in porosity.

Introduction

Combustion of fossil fuels such as oil, natural gas, and coal currently generates in excess of 27 billion tonnes of carbon dioxide per year worldwide,[1] virtually all of which is discharged into the earth's atmosphere. Because of the expanded use of fossil fuels, the atmospheric concentration of CO2 has risen from preindustrial levels of 280 ppm (parts per million) to present day values of approximately 365 ppm.[2] The Intergovernmental Panel on Climate Change (IPCC) has projected that for a “business as usual” energy scenario the atmospheric concentrations of CO2 may double by the middle of the 21st century, and may continue to rise at increasing rates beyond.[3] Atmospheric CO2 is a "greenhouse gas," so-called because it traps outgoing infrared and thermal radiation, thereby increasing near-surface temperatures. There is some evidence from climate modeling that increased atmospheric concentrations of CO2 may be the chief contributor to "global warming," currently estimated to amount to 0.3 - 0.6 ˚C during the last 150 years.[4]

The U.S. Department of Energy (DOE) and other organizations have initiated broad technology programs to assess and develop methods for reducing atmospheric emissions of CO2 (DOE, 1999). One of the more promising concepts involves disposal of CO2 into geologic formations, including oil and gas reservoirs, coal beds, and saline aquifers. CO2 injection into oil and gas reservoirs, and methane-bearing coal beds, can provide collateral benefits in terms of enhancing recovery of oil and natural gas. Saline aquifers are attractive as CO2 disposal reservoirs because they are generally unused and are available in many parts of the U.S. Geologic disposal of CO2 into aquifers would be made at supercritical pressures, in order to avoid adverse effects from CO2 separating into liquid and gas phases in the injection system. The critical point of CO2 is at P_{crit} = 73.82 bar, T_{crit} = 31.04 ˚C,[5] so that minimum aquifer depths of approximately 800 m would be required to sustain a supercritical pressure regime. Injection of CO2 into such aquifers would give rise to the evolution of a two-phase fluid system, in which most of the injected CO2 will reside in a dense supercritical gas phase, while partially also dissolving into the aqueous phase, and reacting with native minerals. From an engineering perspective, the main issues for CO2 disposal in aquifers relate to (1) the rate at which CO2 can be disposed, (2) the

available storage capacity (ultimate CO2 inventory), (3) the presence of a caprock of low permeability, and the potential for CO2 leakage through imperfect confinement, which may be natural or induced, (4) identification and characterization of suitable aquifer formations and caprock structures, (5) uncertainty and possibility of failure due to incomplete knowledge of subsurface conditions and processes, and (6) corrosion resistance of materials to be used in injection wells and associated facilities.

CO2 disposal in aquifers has been discussed in the technical literature since the early 90s.[6-14] There is an obvious analogy to natural gas storage in aquifers, a mature technology that is widely applied in the northeastern U.S.[15] While there is considerable experience with underground injection of CO2 for enhanced oil recovery,[16] the Sleipner Vest project in the Norwegian sector of the North Sea is the only practical example of CO2 disposal into an aquifer.[17,18] Flow systems that involve water, CO2, and dissolved solids have been extensivley studied in geothermal reservoir engineering.[19-22] The geothermal work mostly addresses higher temperatures and lower CO2 partial pressures than would be encountered in aquifer disposal of CO2; some of it involves not only multiphase flow but also chemical interactions between reservoir fluids and rocks.[23]

The amounts of CO2 that would need to be disposed of at fossil-fueled power plants are very large. A coal-fired plant with a capacity of 1,000 MWe (electric) generates approximately 30,000 tonnes of CO2 per day.[14] Large-scale injection of CO2 into aquifers will induce a range of strongly coupled physical and chemical processes, including multiphase fluid flow, changes in effective stress, solute transport, and chemical reactions between fluids and formation minerals. The displacement of aquifer water by CO2 is subject to hydrodynamic instabilities, including viscous fingering and gravity override,[24,13] which may give rise to bypassing and preferential flow along localized pathways, with important impacts, favorable as well as unfavorable, on CO2 containment and storage capacity. Fluid pressures will rise as CO2 displaces aquifer water in which it partly dissolves. CO2 dissolution will lower the pH of the aqueous phase, and will give rise to chemical interactions with aquifer minerals. Dissolution of primary and precipitation of secondary minerals will alter formation porosities and permeabilities. Continuous injection of CO2 will lead to increased formation pressures over large areas, of the order of 100 km^2 or more, which will modify the local mechanical stress field, causing deformation of the aquifer.

This paper discusses the capacity of saline aquifers to store injected CO2 either as a free gas-like phase, or dissolved in the aqueous phase, or bound to solid minerals. Storage capacity factors are estimated using volumetric averages, as well as on the basis of frontal displacement theory, and numerical simulation.

Capacity factor

As discussed above, CO2 injected into an aquifer can be present in several different storage modes, namely, (1) in a CO2-rich gas-like phase, (2) dissolved in the aqueous phase, and (3) immobilized in solid minerals, which form as injected CO2 reacts with the pre-existing mineral assemblage. In order to evaluate and compare the different CO2 sequestration mechanisms we need a convenient general measure of the relative contributions of CO2 storage in gas, aqueous, and solid phases. To this end we introduce the "capacity factor" (CF) of the formation, which may be loosely defined as the fraction of aquifer pore volume that is accessible to CO2. Denoting the CO2-rich phase as "gas," the aqueous phase as "liquid," and the assemblage of mineral phases as "solid," the total mass of CO2 present in a reservoir volume V can be written as a sum over the phases,

$$M^{CO2} = M_g^{CO2} + M_l^{CO2} + M_s^{CO2} \qquad (1)$$

A useful quantitative measure for capacity factor CF can be defined by comparing M^{CO2} with the mass of CO2 that could be stored in that same reservoir volume V if the entire pore space were filled with gas-like CO2 at the same temperature and pressure conditions. Denoting this hypothetical mass of CO2 by $M_{all\,gas}$, we have

$$M_{all\,gas} = V\phi\rho_g(T,P,X) \qquad (2)$$

where ϕ is porosity, and ρ_g is gas density, which depends on temperature, pressure, and gas composition (CO2 mass fraction X). Here and in what follows we neglect the small contribution of water vapor to gas density, and we assume that injected gas is pure CO2, so that X = 1. Combining Eqs. (1, 2) we define the "capacity factor" as

$$\begin{aligned} CF &= M^{CO2}/M_{all\,gas} \\ &= CF_g + CF_l + CF_s \end{aligned} \qquad (3)$$

where the contributions of the individual phases are given by

$$\begin{aligned} CF_g &= \bar{S}_g \\ CF_l &= \bar{S}_l\,\bar{\rho}_l\,\bar{X}_l^{CO2}/\bar{\rho}_g \\ CF_s &= \bar{v}_s\,\bar{\rho}_s\,\bar{X}_s^{CO2}/\phi\,\bar{\rho}_g \end{aligned} \qquad (4)$$

Here, S_β (β = g, l) is the saturation of phase β, ρ_β is density, X_β^{CO2} is the mass fraction of CO2 in phase β, and v_S is the fraction of reservoir volume occupied by solid phases that chemically fix CO2. Overbars indicate appropriate volume averages. The individual phase contributions CF_β (β = g, l, s) to total capacity factor can be interpreted as the gas phase saturations that would be required to store an equivalent

amount of CO2 at prevailing temperature and pressure conditions. CF_g is equal to $\bar{S}_g$, the average gas saturation in the storage volume. Note that CF_g and CF_l depend on phase saturations but not on porosity. As will be seen below, reasonable estimates of phase saturations expected for aquifer disposal of CO2 can be easily made, so that CF_g and CF_l allow a robust comparison of the CO2 storage in gas and liquid phases. When comparing the sequestration capacity of solid minerals with that of fluid phases it is not possible to avoid a dependence on the ratio of sequestering mineral volume to pore volume, v_s/ϕ, making CF_s less useful as a general measure of sequestration capacity.

During a CO2 disposal operation, the various components of CF will be affected by transient, steady-state, and equilibrium effects. Immiscible displacement of water from injected CO2 to establish a gas-filled pore space occurs on a rapid time scale, reflecting actual injection rates and their temporal variations. Dissolution of gaseous CO2 into the aqueous phase is subject to equilibrium solubility locally, but may occur relatively slowly on a reservoir scale, as it must proceed, in part, by diffusion of dissolved CO2 to regions that may be bypassed by the advancing CO2 front. Sequestration of CO2 by precipitation of secondary minerals tends to be a slow process at the temperature conditions expected for aquifer disposal of CO2, requiring tens or hundreds of years for substantial reaction progress at temperatures of 40 - 70 °C.[25,26]

Below we present simple models to obtain a first semi-quantitative outlook on the different components of capacity factor, so that the relative importance of CO2 storage in gas, aqueous, and solid phases may be evaluated. Our analysis uses a previously developed fluid property model for supercritical CO2 and CO2-water mixtures[27] and a reactive geochemical transport model TOUGHREACT.[28]

Gas phase. Extensive studies of the PVT properties of CO2 have been carried out in the former Soviet Union.[5,29-32] We use the correlations developed by Altunin,[30] as implemented in a computer program kindly provided to us by Victor Malkovsky of IGEM, Russia (private communication 1999). Altunin's correlations were extensively cross-checked and found to represent density, viscosity, and enthalpy of pure CO2 within experimental accuracy for the pressure and temperature conditions of interest here.[27] Fig. 1 shows density and viscosity of CO2 at supercritical pressures.

For the conditions shown in Fig. 1, CO2 viscosity is lower than the viscosity of pure water by factors ranging from 10 - 40; the viscosity contrast is even larger in comparison to brines. Injection of CO2 into a water-filled porous medium is therefore subject to hydrodynamic instabilities. From the analysis given in ref. 24, the wavelength λ_m of maximum fingering instability can be estimated as

$$\lambda_m^2 = \frac{12\pi^2 k}{N_c^*} \qquad (5)$$

where k is formation permeability, and $N_c^* = \mu_w u/\sigma^*$ is a capillary number, with μ_w the water viscosity, u the volumetric flux (Darcy velocity), and σ^* an effective interfacial tension. In writing Eq. (5) we have neglected the inverse fluid mobility μ_g/k_{rg} for CO2 as small in comparison to that of the aqueous phase. In field injection systems we expect capillary numbers in the range of from 10^{-3} to perhaps as low as 10^{-10},[35] which corresponds to wavelengths for fingering in the range of .3 mm $\le \lambda_m \le$ 1.08 m. This estimate suggests that fingering from hydrodynamic instabilities will not be a significant issue for field-scale problems. Instead, the heterogeneity structure of the aquifer will determine the extent to which CO2 is channeled into higher-permeability pathways while bypassing regions of lower permeability.

A useful estimate of gas phase capacity factor can be obtained by ignoring issues of hydrodynamic instability and reservoir heterogeneity, and also neglecting effects of capillarity and CO2 compressibility, and neglecting two-dimensional flow effects due to CO2 buoyancy. Under these approximations the advance of the gas displacement profile is given by the Buckley-Leverett solution.[33] Gas saturations depend on injected volume V_{inj} and time only through V_{inj}/t, so that the average gas saturation in the swept region is time independent. The gas phase capacity factor is given by

$$CF_g = \bar{S}_g = S_f/f_f \qquad (6)$$

where S_f and f_f are gas saturation and fractional flow of gas phase, respectively, at the displacement front.[34,35] Actual values for CF_g depend on fractional flow characteristics, i.e. on relative permeability behavior and fluid viscosities.

For typical conditions of T = 40 °C and an aqueous phase viscosity of .8e-3 Pa.s, we have evaluated Eq. (6) for a range of CO2 viscosities and a variety of porous media. Relative permeabilities were assumed as follows.

$$k_{rl} = \sqrt{S^*}\left\{1-\left(1-[S^*]^{1/m}\right)^m\right\}^2 \qquad (7a)$$

$$k_{rg} = \left(1-\hat{S}\right)^2\left(1-\hat{S}^2\right) \qquad (7b)$$

where $S^* = (S_l - S_{lr})/(1 - S_{lr})$, $\hat{S} = (S_l - S_{lr})/(1 - S_{lr} - S_{gr})$. Eq. (7a) for liquid was developed by van Genuchten;[36] Eq. (7b) for gas is due to Corey.[37]

Table 1 summarizes data in order of decreasing permeability (k) of the geologic media. Parameters for wetting phase

relative permeability include irreducible water saturation S_{lr} and pore size distribution index m. Gas phase irreducible saturation was assumed as S_{gr} = .05 throughout. From these parameters we derive frontal saturation S_f, fractional flow f_f, and gas phase capacity factor CF_g, which is equal to average saturation $\overline{S}_g$ in the swept region. Hydrogeologic data (k, S_{lr}, m) identified by texture (sand, loam, etc.) were taken from a tabulation of soil properties,[38] while data labeled with formation names pertain to sedimentary formations at the Hanford site, Columbia Plateau, Washington (Yabusaki, private communication, 2000).[39] The reason for selecting the media listed in Table 1 is simply that absolute and relative permeability data were conveniently available, so that gas phase capacity factors could be estimated for a range of parameters that are of interest for aquifer disposal of CO2.

The data in Table 1 show a systematic trend with permeability, and appear to be quite consistent between the various types of soils and sediments. Gas phase capacity factors range from approximately 40 % for media with large permeabilities (> 1 darcy), to below 20 % for less permeable media. Capacity factors generally become smaller for finer textured and less permeable media. A larger viscosity contrast (smaller CO2 viscosity at lower pressure, see Fig. 1b) also results in smaller gas phase capacity factors.

We emphasize that the gas phase capacity factors obtained above apply to uniformly swept media. If formation heterogeneities and/or buoyancy effects would cause significant bypassing then capacity factors would be further reduced (see below).

Liquid (aqueous) phase. We consider sodium chloride (NaCl) brine. Following ref. 21, aqueous phase (brine) density is calculated as a function of temperature, pressure, and salinity from correlations given in refs. 20, 40. Brine viscosity is obtained from a correlation given in ref. 41. Ref. 21 indicates that these correlations agree well with published experimental data. Halite solubility is calculated from an equation due to Potter;[42] effects of dissolved CO2 concentration on halite solubility are small (a few percent[43]) and have been neglected. Salinity effects on vapor pressure are represented with the correlation given in ref. 40. At present no allowance is made for a dependence of brine density and viscosity on dissolved CO2.

Dissolution of CO2 is represented by an extended version of Henry's law which includes salinity effects and fugacity corrections for CO2 solubility.[44]

$$\Phi P_n = K_h x_n \qquad (8)$$

Here, P_n and x_n are, respectively, the pressure and dissolved mole fraction of the non-condensible gas, Φ (< 1) is the fugacity coefficient, which depends on temperature and pressure, $\Phi = \Phi(T, P_n)$, and $K_h = K_h(T, x_S)$ is Henry's coefficient, which is a function of temperature T and mole fraction x_S of solid ("salt") dissolved in the aqueous phase. For F we use the correlation developed in ref. 45 which is accurate in the range 50 °C ≤ T ≤ 350 °C, and 0 ≤ P_n ≤ 500 bars; at T = 40 °C errors can be as large as 10 %. The temperature and salinity dependence of Henry's coefficient is represented using the correlations developed in ref. 21. Pruess and García[27] found that these agree well with correlations developed by Xu, whose temperature dependence was obtained from the EQ3/6 database,[46] and whose salinity dependence was derived from activity coefficients presented in ref. 47.

We have used Eqs. (4, 8) to estimate liquid phase capacity factors CF_l for a range of conditions most likely encountered in aquifer gas storage, namely, temperatures: 35 - 100 °C, pressures: 80 - 450 bars, and salinity from small values all the way to saturated NaCl brines. In order to make these estimates we assume a representative gas saturation of 20 % in the region swept by injected CO2. Gas saturation enters in the form (1-S_g), so that CF_l is not very sensitive to gas saturations as long as these are substantially smaller than liquid saturations, $S_g << S_l$. Pressure dependence of CF_l enters primarily through the dissolved mass fraction $\overline{X}_l^{CO2}$ and gas density $\overline{\rho}_g$. For an ideal gas and ideal solution at low pressures, both $\overline{X}_l^{CO2}$ and $\overline{\rho}_g$ will be proportional to pressure, so that overall pressure dependence of CF_l would be weak (through $\overline{\rho}_l$ only). CO2 fugacities decrease with increasing pressures, so that the increase of $\overline{X}_l^{CO2}$ with pressure will be more modest. At the same time, real gas effects will reduce the increase of gas density with pressure. These effects tend to compensate each other, leading to a very weak dependence of CF_l on pressure, see Fig. 2.

The temperature dependence of CF_l is also subject to compensating effects between $\overline{X}_l^{CO2}$ and $\overline{\rho}_g$. Henry's coefficient for CO2 increases with temperature, up to a maximum that is reached near 180 °C,[27] so that both $\overline{X}_l^{CO2}$ and $\overline{\rho}_g$ decrease with temperature. Fig. 3 shows that CF_l varies with temperature by less than one percentage point for 35 °C ≤ T ≤ 100 °C. A stronger dependence occurs for salinity, because Henry's coefficient increases by approximately a factor 3 from pure water to saturated NaCl solutions.[27] This "salting out" effect causes CF_l to decrease by a similar factor, see Fig. 4.

In summary, we can state that for conditions of interest in aquifer disposal of CO2 the liquid phase capacity factor CF_l is only weakly dependent on CO2 pressure and temperature. It also depends weakly on gas saturation as long as $S_g << S_l$. For pressures between 100 and 450 bars, and temperatures between 40 °C and 100 °C, CF_l for a brine with 10 % mass fraction of NaCl is in the range of from 5 - 6 %. For the

assumed gas saturation of 20 %, therefore, CO2 storage in the liquid phase amounts to approximately 1/4 of the amount stored as gas. CF_l depends strongly on salinity, ranging from 2 % in saturated NaCl brines to 7 % for dilute waters.

Solid phases. Carbon dioxide (CO2) can react directly or indirectly with certain minerals in a geologic formation leading to the precipitation of secondary carbonates. This process is called "mineral trapping",[9] which is potentially attractive because it could immobilize CO2 for long time scales, and prevent its easy return to the atmosphere. Sequestration of carbon dioxide in subsurface rock formations depends on the availability and quantities of metal oxide components that can react with carbon dioxide to form solid carbonates with low solubility. Only a limited suite of rock forming chemical components possesses the required properties. They include MgO, CaO, MnO, FeO, SrO and BaO. FeO and MnO are stable only under reducing conditions at low temperatures, such as might occur in buried sedimentary rocks containing organic residues. However, it should be noted that organic matter can also reduce sulfate ion to HS^-, which competes with dissolved carbonate species to precipitate ferrous sulfides. The alkali earth metal oxides, CaO, SrO and BaO can also form low-solubility sulfates, the relative stability of the carbonate or sulfate being determined by the potentials of CO2 or SO3 in a given environment.

We surveyed all major classes of rock-forming minerals whose alteration would lead to carbonate precipitation. Table 2 lists some major mineral classes and specifies the maximum quantity of carbon dioxide that could be sequestered by each mineral, assuming complete alteration of the primary minerals. Actual sequestration capacity depends on the geochemical conditions and on the relative abundance of the various primary minerals. A more extensive list is reported in ref. 48. The most suitable aquifer host rocks are sandstones, whose principal constituent, quartz, is chemically inert to CO2. Sandstones generally contain only minor quantities, i.e. less than 10 wt.%, of those primary detrital minerals such as plagioclase, pyroxene, amphibole or chlorite that would alter and form secondary carbonate minerals. Primary or secondary clay minerals such as illite or smectite, which would be destabilized in the presence of dissolved CO2, have relatively small carbonate sequestration capacities (Table 2). Furthermore, concentrations of clay in excess of 15 wt.%, degrade the permeability and porosity of sandstones, making them unsuitable for CO2 disposal.

In order to put the numbers listed in Table 2 in perspective, let us compare them with the amount of CO2 that may be stored in the gas phase, which we expect to be of order $CF_g \approx 0.2$. We consider that a fraction v_S = 1 % of the reservoir volume contains a CO2-consuming mineral. Assuming a porosity of ϕ = .12, and a gas phase CO2 density of 781.2 kg/m^3 (corresponding to T = 40 °C, P = 150 bar), the coefficient $v_S/\phi\bar{\rho}_g$ to be applied to convert the data in Table 2 to an equivalent gas phase saturation CF_S is 1.07e-4. This means that a sequestration potential of 1,000 kg/m^3 in Table 2 corresponds to CF_S = 10.7 %, a figure which is about half of the expected capacity factor for CO2 storage in the gas phase.

Numerical simulations

The large scale of aquifer perturbations that would arise from CO2 disposal can be appreciated by considering the representative case of a standard-size 1,000 MW coal-fired power plant. This produces CO2 at a rate of approximately 350 kg/s (≈ 30,000 tonnes per day[14]), so that the total amount of CO2 that would need to be disposed over an assumed project life of 30 yr would be 3.31e11 kg. Based on the analyses presented above we estimate the combined capacity factor for gas and liquid phase storage as $CF_g + CF_l \approx .25 + .05 = .30$, and neglect contributions from mineral sequestration as insignificant (too slow) over a 30 year period. The amount of CO2 stored per unit reservoir volume in the region swept by the injection plume is $\phi(CF_g + CF_l)\rho_g$, where ρ_g represents a typical in situ density of order 800 kg/m^3 (at T = 40 °C, P = 163.1 bar). Assuming a porosity of ϕ = 12 % as may be typically encountered in a disposal aquifer,[15] CO2 storage is estimated at 28.8 kg per unit reservoir volume. This CO2 would reside in a reservoir volume of 3.31e11/28.8 = 1.15e10 m^3. If average vertical thickness of the aquifer is H = 100 m, the CO2 plume would extend over an area of 115 km^2.

These estimates were evaluated by means of numerical simulation, using our general-purpose multiphase flow simulator TOUGH2[49] and the fluid property description discussed above. We assume the aquifer to be infinite-acting and homogeneous, and neglect inertial and non-isothermal effects. Our simulation includes effects of salinity on density and viscosity of the aqueous phase, as well as salinity and fugacity effects on CO2 dissolution. The well field is modeled as a circular region of R = 1 km radius into which CO2 is injected uniformly at a constant total rate of 350 kg/s. A 2-D R-Z grid was used, and three cases were run with different vertical permeability. Parameter specifications were chosen representative of conditions that may be encountered in brine aquifers at a depth of order 1 km, see Table 3.

The case with $k_V = 0$ corresponds to 1-D radial flow. Except for effects from the finite-size injection region, the 1-D radial flow problem admits a similarity solution which depends on radial distance and time only through the similarity variable $\xi = R^2/t$.[19] This holds true even when taking into account all of the non-linearities due to PVT properties (density, viscosity, and phase partitioning effects) and due to two-phase flow (relative permeability and capillary pressure). Fig. 5 shows results for fluid pressure, gas saturation, and dissolved CO2 mass fraction as a function of the similarity variable, confirming the similarity property through the excellent agreement between time-dependent data at a fixed distance, and a radial profile at a fixed time.

Contour plots of gas saturation for the two anisotropic cases are shown in Fig. 6, and Table 4 gives a summary of results for different anisotropy. For larger vertical permeability there obviously is more CO2 migration towards the top of the aquifer, and more of the deeper regions are bypassed. This results in an increased areal extent of the CO2 plume, less CO2 stored per unit reservoir volume in the region swept by the plume, and reduced gas and liquid phase storage capacity. The reduction in the fraction of aquifer volume available for CO2 storage due to buoyancy effects is partially compensated by the fact that gas saturations in the CO2 plume increase as bypassing effects become stronger. These compensating effects explain why the estimates of CO2 storage capacity obtained above from 1-D frontal displacement theory remain reasonable and useful even when buoyancy gives rise to 2-D flow effects. A consequence of increased bypassing for larger vertical permeability is that more of the CO2 injected is stored in the gas phase and less is dissolved in water. The accumulation of CO2 at the top of the aquifer seen for larger vertical permeability leads to more segregated flow, with reduced phase interference effects, and much reduced wellfield pressures.

Geochemical modeling

Numerical modeling of geochemical processes is a necessary predictive tool for long-term CO2 disposal in deep aquifers, because alteration of the predominant host rock aluminosilicate minerals is very slow and is not experimentally accessible under ambient deep-aquifer conditions. To analyze the impact of CO2 immobilization through carbonate precipitation, we performed batch reaction modeling of several different aquifer mineralogies using the code TOUGHREACT.[28] Below, we report the setup and results for a glauconitic sandstone aquifer from the Alberta Sedimentary Basin (Canada) that had been studied previously.[26] Modeling results for two additional rock types (Gulf Coast sediments, and dunite) are given in ref. 48.

The glauconitic aquifer has an average mineral composition of 87% quartz, 2% potassium-feldspar, 1% plagioclase, 5% glauconite, 2% kaolinite, 1% calcite, 1% dolomite, and 1% siderite. The average porosity is 12%. Gunter et al. (1997) modeled water-rock reactions driven by the formation of carbonic acid when CO2 is injected into deep aquifers using PATHARC.94.[50] In their simulations, the CO2 injection pressure was set at 260 bar. Annite was used as a substitute for glauconite, which is the trioctahedral ferrous iron end-member mineral ($KFe_3AlSi_3O_{10}(OH)_2$) of the phlogopite-annite series. Plagioclase was simulated by assuming the presence of discrete fractions of end member components, anorthite and albite. In the present study, we initially assumed the same mineralogy as ref. 26 and obtained similar results. Our simulation shows that annite is rapidly destroyed with precipitation of siderite ($FeCO_3$), the latter being the principal mineral trap for CO2. A maximum of about 40 kg of CO2 per m^3 of host rock medium can be sequestered as carbonates.

The use of annite as a substitute for glauconite overestimates the availability of Fe2+, the amount of siderite ($FeCO_3$) precipitation, and hence the degree of CO2 sequestration. To rectify this, we estimated the thermodynamic parameters for glauconite with a representative chemical composition. We also incorporated oligoclase as a solid solution of plagioclase. Also, instead of using muscovite as a proxy for illite, we assumed that illite was actually present as a primary mineral. Furthermore, we assumed that organic matter, represented by the generic composition, CH_2O, was present in the glauconitic sandstone. This allowed us to consider processes involving redox sensitive pairs such as Fe3+/Fe2+, CO2(aq)/CH4(aq), H2O(aq)/H2(aq) and SO_4^{2-}/HS-, which could vary during the chemical evolution of the system. The decomposition of organic matter is a complex process. A more realistic representation of organic matter should be investigated in the future. The mineralogical composition in our simulations was modified accordingly to accommodate these additions. We believe the modified mineralogy more accurately represents natural conditions.

Our geochemical simulations consider 1 m^3 water-saturated medium. The initial condition used is a pure 1.0 M solution of sodium chloride reacting with the primary minerals at a temperature of 54 °C, a pH of 7, and an Eh of -0.1 V. The reactant minerals dissolve progressively into the formation water, thus modifying its composition and leading to precipitation of product phases. Mineral dissolution and precipitation is considered to be kinetically controlled. A first order kinetic rate law was used.[51] The rate law parameters and reactive surface areas used can be found in ref. 48. Two simulations were performed. The first simulation was for water-rock interaction under natural conditions without CO2 injection (background case). However, some CO2 is generated from the decomposition of organic matter and may subsequently be fixed as carbonates. The second simulation considers CO2 injection under a pressure of 260 bar. This pressure is the same as that chosen in ref. 26 for the glauconitic sandstone aquifer, and is based on the assumption that the aquifer is 1500 m deep, and can sustain CO2 disposal injection pressures of that magnitude.

For the simulation without CO2 injection, an approximately constant pH of 7 and an Eh of -0.16 V are achieved after 12,000 years. Both CO2 and CH4 are generated at different periods during the simulations (Fig. 7). In the present simulations, we consider only the aqueous CO2 and CH4 species. However, we calculated the corresponding gaseous partial pressures indirectly according to mass-action equation. After 10,000 years, CH4 appears and CO2 disappears. The distribution of mineral abundances is presented in Fig. 8. Oligoclase and kaolinite dissolve completely after 4,000 years, which is unrealistically fast, as complete reaction of these minerals may take millions of years under buried conditions. Organic matter dissolves at a constant rate. Glauconite initially dissolves faster, but eventually slows to a constant rate after 12,000 years. Illite precipitates initially (before 4,000 years), but dissolves after the disappearance of kaolinite. Albite-low

and smectite-Na generally precipitate. K-feldspar initially dissolves, and then precipitates. Calcite and siderite precipitate in minor amounts. Dolomite initially dissolves, and then precipitates. It should be pointed out that the simulation can not achieve chemical equilibrium because organic matter decomposition is strongly kinetically controlled. Equilibrium may be reached only after complete decomposition of organic matter. However, a quasi-steady state (constant mineral dissolution and precipitation rates) is reached after 12,000 years. With the current batch reaction modeling approach (closed system), gas pressures increase continuously over time, which is not realistic. Future work should include full coupling between chemical reactions and fluid flow (open system).

For the simulation with a CO2 injection pressure of 260 bar, a lower pH (about 5) and higher Eh (above 0.15 V) are obtained, both of which are buffered by the CO2 gas pressure. CH4 generation is suppressed because of the higher values of Eh. The distribution of mineral phases is presented in Fig. 9. CO2 injection significantly enhances mineral dissolution and precipitation processes because of the decreased pH. Consequently, glauconite and illite dissolve at much higher rates. Calcite and dolomite precipitate to a limited extent (Fig. 9b). Siderite precipitation is significant because of significant availability of carbonate and rapid glauconite dissolution. The cumulative sequestration of CO2 with time is presented in Fig. 10. Most CO2 is sequestered through siderite (FeCO3) precipitation. Only minor amounts of calcite and dolomite precipitate because both minerals are more soluble. In addition, CO2 injection leads to a considerable decrease in porosity (Fig. 11), because of enhanced precipitation of clay minerals.

Discussion

Capacity for CO2 sequestration by minerals. For the glauconitic sandstone aquifer, our simulation suggests that only small amounts of CO2 are sequestered through precipitation of calcite ($CaCO_3$) and dolomite ($CaMg(CO_3)_2$) because both minerals are fairly soluble. In contrast, a significant amount of CO2 is trapped by precipitation of siderite ($FeCO_3$) provided that the Fe3+ component is reduced by organic matter. The total amount of CO2 trapped in mineral phases could reach about 15 kg per m^3 of medium, which is greater than that dissolved in the aqueous phase (less than 10 kg per m^3 of medium). The precipitation of siderite is conditioned by the redox state of the system. However, even relatively low partial pressures of H2S would favor the fixation of Fe2+ as pyrite. This may considerably decrease CO2 sequestration in mineral phases. For Gulf Coast sediments, the only CO2 trapping mineral to appear is calcite which could reach 13 kg per m^3 of medium. Dunite (olivine) would have the largest capacity for CO2 sequestration. One m^3 of dunite could sequester as much as 100 kg CO2 as secondary carbonates. Theoretically, a much higher amount (Table 2) can be sequestered because forsterite and fayalite are still abundant after this time. However, the rock alteration would terminate when the porosity had declined to a negligible value. In addition, this type of rock is not found in significant amounts in the earth's crust. From our analysis, we note that mineral trapping of CO2 varies considerably with rock type. The trapping capabilities also depend on other factors such as gas pressure, temperature, porosity and mineral composition. For the glauconitic sandstone case, the sequestration capacity is proportional to abundances of both glauconite and organic matter. In all three cases we simulated, mineral-trapping capacity is comparable with, and can be larger than that of solubility trapping (about 7-10 kg per m^3 of medium).

Changes in porosity. All three examples demonstrate that rock alteration after CO2 injection results in decreased porosity. This is because (1) CO2 mass is added to the solid matrix, and (2) some altered mineral products have lower densities, such as clay minerals. A small decrease in porosity can result in a significant decrease in permeability. The decrease could reduce the CO2 injectivity. The change in porosity is therefore a very important issue for CO2 injection into deep geologic formations. In ref. 52 a decreasing injectivity during CO2 injection for enhanced oil recovery was observed.

Time required for sequestration. The time frame for CO2 sequestration by minerals is of the order of tens to thousands of years or more and is a function of reaction kinetics. Kinetic rates for rock-fluid system cannot be reliably modeled at present. Sensitivity simulations show that scaling surface areas by the same constant factor is equivalent to scaling the time coordinate and otherwise does not lead to different results. The surface area changes lead to reciprocal changes in the time scale. Specific changes in the reactive surface area for redox sensitive minerals such as glauconite or organic matter significantly affect mineral alteration, and the extent of CO2 sequestration.

Concluding remarks

CO2 injected into aquifers can be stored (1) in a gas-like CO2-rich phase, (2) dissolved in the aqueous phase, and (3) chemically bound in solid minerals. We have defined capacity factors $CF_{g,l,s}$ for gas, liquid and solid phase storage, respectively, and have made preliminary evaluations of sequestration capacity, using volumetric estimates as well as numerical simulation. Gas phase capacity factor is equal to the gas saturation required to store the same mass of CO2 at the same temperature and pressure conditions, and was estimated from 1-D frontal displacement theory (Buckley-Leverett) as typically in the range of 20 - 30 %. Liquid phase capacity factor depends only weakly on temperature and pressure, and varies with salinity from 2 % (saturated NaCl brines) to 7 % (dilute waters).

At the temperature and pressure conditions of interest, the CO2-rich gas-like phase is less dense than water. Depending on the ratio of vertical to horizontal permeability, CO2 has a tendency to migrate upward towards the top of the aquifer, leading to partially segregated flow with considerable bypassing of water (gravity override). These effects are not

included in our simple estimations of CO2 sequestration capacity from 1-D frontal displacement theory. However, by comparing with numerical simulations that include buoyancy effects it was found that the estimates based on 1-D displacemement give a reasonable approximation. This is because gravity override gives rise to increased gas saturations near the top of the aquifer, which partially compensates for the reduction of aquifer volume contacted by CO2, so that effects on the areal extent of the CO2 plume and on volume-averaged gas and liquid storage capacities are relatively modest. Although partial segregation of flow from buoyancy effects leads to some reductions in available CO2 storage capacity, it has one large effect that is favorable. Namely, there is less interference between gas and liquid phases, leading to a considerable reduction in CO2 injection pressures for a given flow rate.

CO2 sequestration by matrix minerals varies considerably with rock type. It is expected to be a slow process with small impacts during the operational life of a CO2 disposal scheme. Under favorable conditions the amount of CO2 that may be sequestered by precipitation of secondary carbonates is comparable with and can be larger than CO2 dissolution in pore waters. The precipitation of siderite ($FeCO_3$) is sensitive to the rate of reduction of ferric mineral precursors such as glauconite, which in turn is dependent on the reactivity of associated organic material. The accumulation of carbonates in the rock matrix, and induced rock mineral alteration due to the presence of dissolved CO2 leads to a considerable decrease in porosity. For typical conditions expected in aquifer disposal of CO2, the total amount of CO2 that may be stored in gas, liquid, and solid phases is of the order of 30 kg per m^3 of aquifer volume.

Nomenclature

c	= compressibility, Pa^{-1}
CF	= capacity factor for CO2 (defined in text)
f	= fractional flow
f_f	= fractional flow at the front
k	= permeability, m^2
k_r	= relative permeability
K_h	= Henry's coefficient
m	= pore size distribution index
M	= mass, kg
M^{CO2}	= mass of CO2, kg
N_c^*	= capillary number
P	= pressure, Pa (10^5 Pa = 1 bar)
R	= radial distance, m
S	= saturation
S_{gr}	= irreducible gas saturation
S_{lr}	= irreducible liquid saturation
t	= time, s
T	= temperature, ˚C
u	= volumetric flux (Darcy velocity), m/s
v	= volume fraction
V	= volume, m^3
x	= mole fraction
X	= mass fraction
X^{CO2}	= mass fraction of CO2
λ	= wave length, m
μ	= viscosity, Pa.s
ϕ	= porosity
Φ	= fugacity
ρ	= density, kg/m^3
σ^*	= interfacial tension, N/m

Subscripts

f	= front
g	= gas phase
h	= horizontal
inj	= injected
l	= liquid (aqueous) phase
m	= maximum
n	= non-condensible gas
s	= solid phases
v	= vertical
w	= water

Acknowledgements

We are grateful to Victor Malkovsky of IGEM, Moscow (Russia) for kindly providing us with his computer programs of the correlations for CO2 properties by V.V. Altunin. Thanks are due to George Moridis and Eric Sonnenthal for a critical review of the manuscript and the suggestion of improvements. This work was supported by the U.S. Department of Energy through the Office of Basic Energy Sciences and through the National Energy Technology Laboratory (NETL) under Contract No. DE-AC03-76SF00098.

References

1. DOE. Carbon Sequestration Research and Development, D. Reichle et al. (eds.), U.S. Department of Energy Report DOE/SC/FE-1, Washington, DC, 1999.
2. Keeling, C.D. and T.P. Whorf. Atmospheric CO2 Records from Sites in the SIO Air Sampling Network, in: *Trends: A Compendium of Data on Global Change,* Carbon Dioxide Information Analysis Center, Oak Ridge National Laboratory, Oak Ridge, TN, 1998.
3. IPCC (Intergovernmental Panel on Climate Change). *Climate Change 1995: The Science of Climate Change,* J.T. Houghton et al. (eds.), Cambridge University Press, Cambridge, United Kingdom, 1996.
4. Ledley, T.S., E.T. Sundquist, S.E. Schwartz, D.K. Hall, J.D. Fellows, and T.L. Killeen. Climate Change and Greenhouse Gases, *EOS,* Transactions Am. Geoph. Union, Vol. 80, No. 39, pp. 453 - 458, 1999.
5. Vargaftik, N.B. *Tables on the Thermophysical Properties of Liquids and Gases*, 2nd Ed., John Wiley & Sons, New York, NY, 1975.

6. van der Meer, L.G.H. Investigations Regarding the Storage of Carbon Dioxide in Aquifers in The Netherlands, *Energy Convers. Mgmt.,* Vol. 33, No. 5 - 8, pp. 611 - 618, 1992.
7. Gunter W.D., Perkins E.H. and T.J. McCann T.J. Aquifer Disposal of CO2-Rich Gases: Reaction Design for Added Capacity. *Energy Convers. Mgmt.,* Vol. 34, pp. 941 - 948, 1993.
8. Holloway S. and Savage D. The Potential for Aquifer Disposal of Carbon Dioxide in the UK. *Energy Convers. Mgmt.,* Vol. 34, pp. 925 - 932, 1993.
9. Bachu, S., Gunter, W.D. and E.H. Perkins. Aquifer Disposal of CO2: Hydrodynamic and Mineral Trapping. *Energy Convers. Mgmt.,* Vol. 35, pp. 269-279, 1994.
10. Bergman P.D. and Winter E.M. Disposal of Carbon Dioxide in Aquifers in the U.S. *Energy Convers. Mgmt.,* Vol. 36, pp. 523 - 526, 1995.
11. Weir, G.J., S.P. White and W.M. Kissling. Reservoir Storage and Containment of Greenhouse Gases, in: K. Pruess (ed.), *Proceedings of the TOUGH Workshop '95,* Lawrence Berkeley National Laboratory Report LBL-37200, pp. 233 - 238, Berkeley, CA, 1995.
12. Fyfe, W.S., R. Léveillé, W. Zang, and Y. Chen. Is CO2 Disposal Possible?, in Preprints of Papers Presented at the 212th ACS National Meeting, pp. 1433 - 1435, American Chemical Society, Orlando, FL, August 25 - 29, 1996.
13. Law, D.H.S. and S. Bachu. Hydrogeological and Numerical Analysis of CO2 Disposal in Deep Aquifers in the Alberta Sedimentary Basin, *Energy Convers. Mgmt.,* Vol. 37, No. 6 - 8, pp. 1167 - 1174, 1996.
14. Hitchon, B. (ed.). *Aquifer Disposal of Carbon Dioxide,* Geoscience Publishing, Ltd., Sherwood Park, Alberta, Canada, 1996.
15. Katz, D.L. and R.L. Lee (1990). *Natural Gas Engineering,* McGraw-Hill Publ. Comp., New York, NY.
16. SPE (ed.) CO2 Flooding, Reprint Series No. 51, Society of Petroleum Engineers, Richardson, TX, 1999.
17. Korbøl, R. and A. Kaddour. Sleipner Vest CO2 Disposal - Injection of Removed CO2 into the Utsira Formation, *Energy Convers. Mgmt.,* Vol. 36, No. 6 - 9, pp. 509 - 512, 1995.
18. Kongsjorden, H., O. Karstad and T.A. Torp. Saline Aquifer Storage of Carbon Dioxide in the Sleipner Project, *Waste Management,* Vol. 17, No. 5/6, pp. 303 - 308, 1997.
19. O'Sullivan, M.J., G.S. Bodvarsson, K. Pruess and M.R. Blakeley. Fluid and Heat Flow in Gas-rich Geothermal Reservoirs, *Soc. Pet. Eng. J.*, 25 (2), 215–226, 1985.
20. Andersen, G., A. Probst, L. Murray and S. Butler. An Accurate PVT Model for Geothermal Fluids as Represented by H2O-NaCl-CO2 Mixtures, *Proceedings 17th Workshop on Geothermal Reservoir Engineering,* pp. 239 - 248, Stanford, CA, 1992.
21. Battistelli, A., C. Calore and K. Pruess. The Simulator TOUGH2/EWASG for Modeling Geothermal Reservoirs with Brines and Non-Condensible Gas, *Geothermics*, Vol. 26, No. 4, pp. 437 - 464, 1997.
22. Moller, N., J.P. Greenberg, and J.H. Weare. Computer Modeling for Geothermal Systems: Predicting Carbonate and Silica Scale Formation, CO2 Breakout and H2S Exchange, *Transport in Porous Media,* Vol. 33, pp. 173 - 204, 1998.
23. Xu, T. and K. Pruess. On Fluid Flow and Mineral Alteration in Fractured Caprock of Magmatic Hydrothermal Systems, *J. Geophys. Res.,* in press, 2000.
24. Chuoke, R.L., P. van Meurs and C. van der Poel. The Instability of Slow, Immiscible, Viscous Liquid-Liquid Displacements in Permeable Media, *Trans. AIME,* Vol 216, pp. 188 - 194, 1959.
25. Perkins, E. H., and Gunter, W. D. A users manual for b PATHARC.94: a reaction path-mass transfer program, Alberta Research Council Report ENVTR 95-11, 179p., 1995.
26. Gunter W.D., B. Wiwchar, and E.H. Perkins. Aquifer Disposal of CO_2-Rich Greenhouse Gases: Extension of the Time Scale of Experiment for CO_2-Sequestering Reactions by Geochemical Modeling. *Mineral. and Petrol.* , Vol. 59, pp. 121 - 140, 1997.
27. Pruess, K. and J. García. Multiphase Flow Dynamics During CO2 Injection into Saline Aquifers, submitted to *Environmental Geology,* September 2000.
28. Xu, T., and Pruess, K. Coupled modeling of non-isothermal multiphase flow, solute transport and reactive chemistry in porous and fractured media: 1. Model development and validation: Lawrence Berkeley National Laboratory Report LBNL-42050, Berkeley, California, 38 p., 1998.
29. Kesselman, P.M. and P.A. Kotlyarovsky. *Thermodynamic Properties of Carbon Dioxide in the Temperature Range from 273-4000 C and Pressures up to 600 bar*, Odessa Technological Institute, 1965.
30. Altunin, V.V. *Thermophysical Properties of Carbon Dioxide,* Publishing House of Standards, 551 pp., Moscow (in Russian), 1975.
31. GSSSD 101-87. *Carbon Dioxide. Coefficients of Dynamic Viscosity, Thermal Conductivity at Temperatures 220-1000 K at Pressures Ranging from Dilute Gas State to 100 MPa*, Tables of Standard Reference Data, Standard Press, Moscow, 1987.
32. Vargaftik, N.B., Y.K. Vinogradov and V.S. Yargin. *Handbook of Physical Properties of Liquids and Gases*,, 3rd Edition, Begell House, 1996.
33. Buckley, S.E. and M.C. Leverett. Mechanism of Fluid Displacement in Sands, *Trans. Am. Inst. Min. Metall. Eng.,* Vol. 146, pp. 107 - 116, 1942.
34. Welge, H.J. A Simplified Method for Computing Oil Recoveries by Gas or Water Drive, *Trans.,* AIME, Vol. 195, pp. 91 - 98, 1952.
35. Willhite, G.P. *Waterflooding,* SPE Textbook Series, Society of Petroleum Engineers, Richardson, TX, 1986.

36. van Genuchten, M.Th. A Closed-Form Equation for Predicting the Hydraulic Conductivity of Unsaturated Soils, *Soil Sci. Soc. Am. J.*, Vol. 44, pp. 892 - 898, 1980.
37. Corey, A.T. The Interrelation Between Gas and Oil Relative Permeabilities, *Producers Monthly*, pp. 38 - 41, November 1954.
38. Carsel, R.F. and R.S. Parrish. Developing Joint Probability Distributions of Soil Water Retention Characteristics, Water Resour. Res., Vol. 24, No. 8, pp. 755 - 769, 1988.
39. Khaleel, R. and E.J Freeman. Variability and Scaling of Hydraulic Properties for 200 Area Soils, Hanford Site, Report WHC-EP-0883, Westinghouse Hanford Company, Richland, WA, October 1995.
40. Haas, J.L. Jr. Physical Properties of the Coexisting Phases and Thermochemical Properties of the H2O component in Boiling NaCl solutions, USGS Bulletin 1421-A, Washington, DC, 73 pp., 1976.
41. Phillips, S.L., A. Igbene, J.A. Fair, H. Ozbek and M. Tavana. A Technical Databook for Geothermal Energy Utilization, Lawrence Berkeley National Laboratory Report LBL-12810, Berkeley, CA, 46 pp., 1981.
42. Chou, I.M. Phase Relations in the System NaCl-KCl-H2O. III: Solubilities of Halite in Vapor-Saturated Liquids Above 445 ˚C and Redetermination of Phase Equilibrium Properties in the System NaCl-H2O, *Geochim. Cosmochim. Acta,* Vol. 51, pp. 1965 - 1975, 1987.
43. Corti, H.R., J.J. de Pablo and J.M. Prausnitz. Phase Equilibria for Aqueous Systems Containing Salts and Carbon Dioxide. Application of Pitzer's Theory for Electrolyte Solutions, *J. Phys. Chem.,* Vol. 94, pp. 7876 - 7880, 1990.
44. Prausnitz, J.M., R.M. Lichtenthaler and E.G. de Azevedo, *Molecular Thermodynamics of Fluid-Phase Equilibria,* 860 p., Prentice Hall, Upper Saddle River, NJ, 2nd ed., 1986.
45. Spycher, N.F. and M.H. Reed. Fugacity Coefficients of H2, CO2, CH4, H2O and of H2O-CO2-CH4 Mixtures: A Virial Equation Treatment for Moderate Pressures and Temperatures Applicable to Calculations of Hydrothermal Boiling, *Geochim. Cosmochim. Acta,* Vol. 52, pp. 739 - 749, 1988.
46. Wolery, T. EQ3/6, A Software Package for Geochemical Modeling of Aqueous Systems: Package Overview and Installation Guide (Version 7.0), Lawrence Livermore National Laboratory Report UCRL-MA-110662 PT1, Livermore, CA 94550, 1992.
47. Drummond, J.M. Jr. Boiling and Mixing of Hydrothermal Fluids: Chemical Effects on Mineral Precipitation, PhD thesis, The Pennsylvania State University, University Park, PA, 1981.
48. Xu, T., Apps, J. A., and Pruess, K. Analysis of mineral trapping for CO2 disposal in deep aquifers, Lawrence Berkeley National Laboratory Report LBNL-46992, Berkeley, California, 2000.
49. Pruess, K., C. Oldenburg and G. Moridis. TOUGH2 User's Guide, Version 2.0, Lawrence Berkeley National Laboratory Report LBNL-43134, Berkeley, CA, November 1999.
50. Perkins, E.H. and W.D. Gunter. Aquifer Disposal of CO2-rich Greenhouse Gases: Modelling of Water-Rock Reaction Paths in a Siliciclastic Aquifer. In Y.K.Kharaka and O.V. Chudaev (eds.), VIIIth International Symposium on Water-Rock Interaction, Balkema, Rotterdam, pp.895-898, 1995.
51. Steefel, C. I., and Lasaga, A. C. A coupled model for transport of multiple chemical species and kinetic precipitation/dissolution reactions with applications to reactive flow in single phase hydrothermal system, *American Journal of Science,* v. 294, p. 529-592, 1994.
52. Ross, G. D., Todd, A. C., Tweedie J. A., and Will, A. G. S. The dissolution effects of CO2-brine systems on the permeability of U.K. and North Sea Calcareous Sandstones, Society of Petroleum Engineers/U.S. Department of Energy Third Joint Symposium on Enhanced Oil Recovery, Paper SPE/DOE 10685, p. 149-154, 1982.

Table 1. Frontal displacement behavior in a variety of porous media.

formation/ texture	k (m^2)	S_{lr}	m	S_f	f_f	CF_g (μ_g = 1.e-4 Pa.s) $	CF_g (μ_g = .25e-4 Pa.s) &
sand	8.25e-12	.105	.6269	.322	.823	.391	.302
loamy sand	4.05e-12	.139	.5614	.293	.828	.354	.276
Hanford backfill	2.48e-12	.0774	.658	.339	.821	.413	.319
sandy loam	1.23e-12	.158	.4709	.260	.833	.312	.246
Hanford formation	1.11E-12	0.0837	.469	.280	.831	.337	.264
Middle Ringold	660.e-15	0.0609	.392	.258	.835	.309	.244
Upper Ringold	474.e-15	.2130	.386	.219	.842	.260	.208
loam	289.e-15	.181	.3590	.217	.842	.258	.207
silt loam	125.e-15	.149	.2908	.199	.848	.235	.190
Plio-Pleistocene	123.e-15	.2595	.456	.228	.839	.272	.216
silt	69.4e-15	.0739	.2701	.204	.847	.241	.195
sandy clay	33.3e-15	.263	.1870	.138	.869	.159	.132

$ corresponding to T ≈ 40 ˚C, P ≈ 337 bar
& corresponding to T ≈ 40 ˚C, P ≈ 83.5 bar; or T ≈ 70 ˚C, P ≈ 111 bar

Table 2. Capacity of different rock-forming minerals to sequester CO2.

Mineral Name	Mineral Formula	Potential CO_2 Fixed, kg/m^3 mineral
Plagioclase (anorthite)	$Ca[Al_2Si_2O_8]$	436.4
Olivine (forsterite-fayalite)	Mg_2SiO_4 - Fe_2SiO_4	2014.7-1896.3
Pyroxene group-enstatite	$(Mg,Fe)_2Si_2O_6$	1404.2
Augite	$(Ca,Mg,Fe(II),Al)_2(Si,Al)_2O_6$	1306.3
Amphibole group-anthophyllite-cummingtonite	$(Mg,Fe(II),Fe(III),)_{5-7}Al_{0-2}[Si_{6-8}Al_{2-0}O_{22}](OH)_2$	1169.5-1041.8
Common hornblende	$Ca_2Na_{0-1}(Mg,Fe(II))_{3-5}(Al,Fe(III))_{2-0}[Si_{6-8}Al_{2-0}O_{22}](O,OH)_2$	1000.4
Calcium amphiboles-tremolite	$Ca_2Na_{0-1}(Mg,Fe(II))_{3-5}(Al,Fe(III))_{2-0}[Si_{6-8}Al_{2-0}O_{22}](O,OH)_2$	1119.3
Mica group-glauconite	$(K,Na,Ca)_{1.2-2.0}(Fe(III),Al,Fe(II),Mg)_{4.0}[Si_{7-7.6}Al_{1-0.4}O_{20}](OH)_4.nH_2O$	61.97
Mica group-phlogopite	$K_2(Mg,Fe(II))_6[Si_6Al_2O_{20}](OH)_4$	881.8
Mica group-biotite	$K_2(Mg,Fe(II))_{6-4}(Fe(III),Al)_{0-2}[Si_{6-5}Al_{2-3}O_{20}](OH)_{4-2}$	671.0
Serpentine	$Mg_6Si_4O_{10}(OH)_8$	1232.7
Chlorite group	$(Mg,Al,Fe(II))_{12}[(Si,Al)_8O_{20}](OH)_{16}$	923.4
Clay minerals-illite	$K_{1-1.5}(Fe(III),Al,Fe(II),Mg)_{4.0}[Si_{7-6.5}Al_{1-1.5}O_{20}](OH)_4$	78.42
Clay minerals-smectite	$(1/2Ca,Na)_{0.7}(Al,Mg,Fe)_4(Si,Al)_8O_{20}(OH)_4.nH_2O$	161.2

Table 3. Hydrogeologic parameters for radial flow problem

Aquifer thickness	H = 100 m
Permeability horizontal	$k_h = 10^{-13}$ m^2
vertical	$k_v = 0, 0.1k_h, k_h$
Porosity	$\phi = 0.12$
Compressibility	$c = 1x10^{-8}$ Pa^{-1}
Temperature	40 ˚C
Pressure	100 bar
Salinity	5 wt.-%
CO2 injection rate	350 kg/s
Relative permeability	
liquid: van Genuchten function[36] $k_{rl} = \sqrt{S^*}\left\{1-\left(1-\left[S^*\right]^{1/m}\right)^m\right\}^2$	$S^* = (S_l - S_{lr})/(1 - S_{lr})$
irreducible water saturation	$S_{lr} = 0.30$
exponent	m = 0.457
gas: Corey curve[37] $k_{rg} = \left(1-\hat{S}\right)^2\left(1-\hat{S}^2\right)$	$\hat{S} = \dfrac{(S_l - S_{lr})}{(1 - S_{lr} - S_{gr})}$
irreducible gas saturation	$S_{gr} = 0.05$
Capillary pressure	
van Genuchten function[36] $P_{cap} = -P_0\left(\left[S^*\right]^{-1/m} - 1\right)^{1-m}$	$S^* = (S_l - S_{lr})/(1 - S_{lr})$
irreducible water saturation	$S_{lr} = 0.0$
exponent	m = 0.457
strength coefficient	$P_0 = 19.61$ kPa

Table 4. Summary of simulated results after 30 years of CO2 disposal from a 1,000 MW coal-fired plant for different levels of anisotropy.

case / parameter	$k_v = 0$ (1-D radial)	$k_v = 0.1\ k_h$	$k_v = k_h$
mass of CO2 stored in gas, kg	2.71e11	2.73e11	2.92e11
gas phase volume, m^3	3.26e8	3.33e8	3.66e8
average CO2 density in gas phase, kg/m^3	831.3	819.8	797.8
mass of CO2 dissolved in water, kg	6.02e10	5.87e10	3.89e10
fraction of CO2 stored in aqueous phase	18.2 %	17.7 %	11.7 %
injection plume area, km^2	89.7	105.7	128.7
average CO2 mass per unit reservoir volume, kg/m^3	36.9	31.3	25.7
CF_g	30.3 %	26.3 %	23.7 %
CF_l	5.5 %	4.7 %	2.8 %
average wellfield pressure, bar	259.3	238.6	190.2

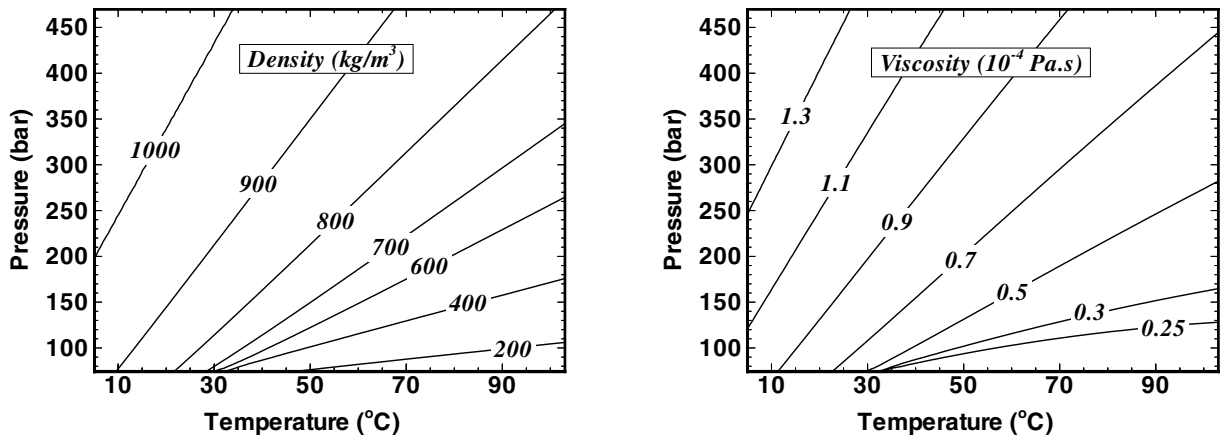

(a) (b)

Figure 1. Contour diagrams of CO2 density (a) and viscosity (b), as calculated from our tabular equation of state based on the correlations of Altunin.[30]

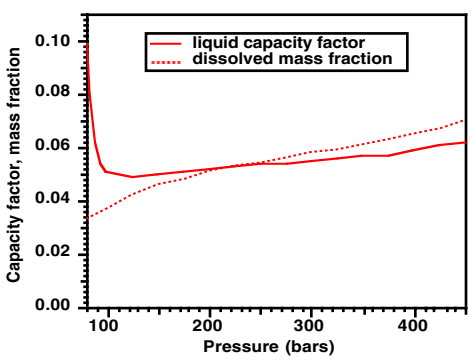

Figure 2. Liquid capacity factor and dissolved CO2 mass fraction at T = 40 ˚C, X_l^{salt} = 10 %.

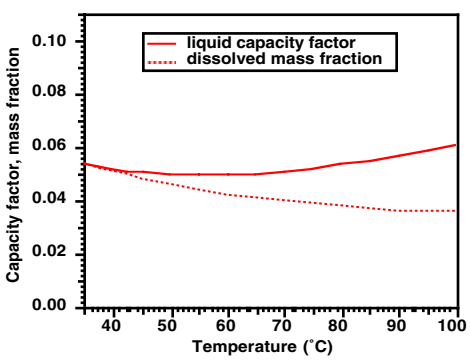

Figure 3. Liquid capacity factor and dissolved CO2 mass fraction at P = 200 bar, X_l^{salt} = 10 %.

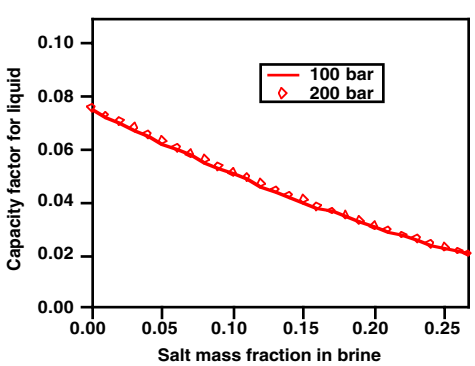

Figure 4. Liquid capacity factor at T = 40 ˚C.

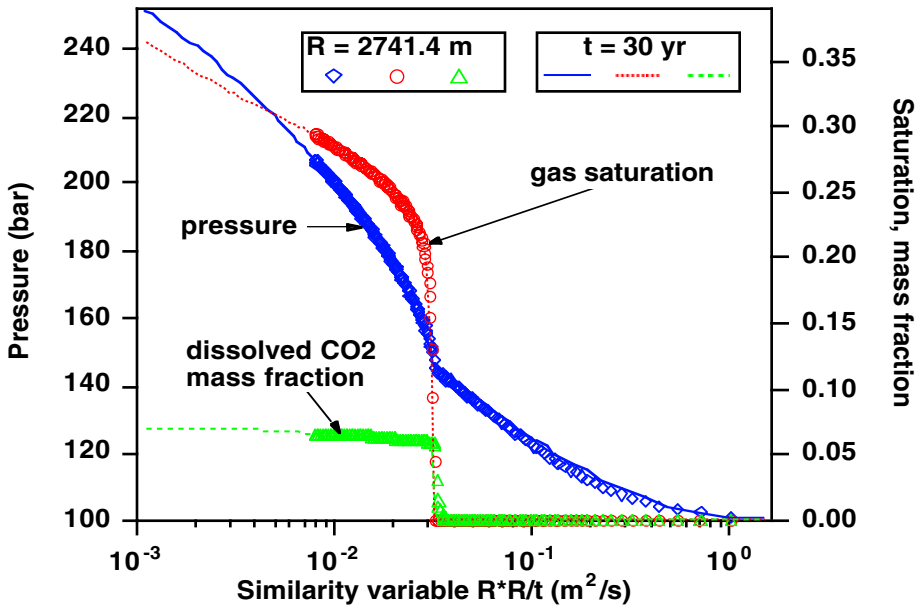

Figure 5. Simulated results for 1-D radial flow problem.

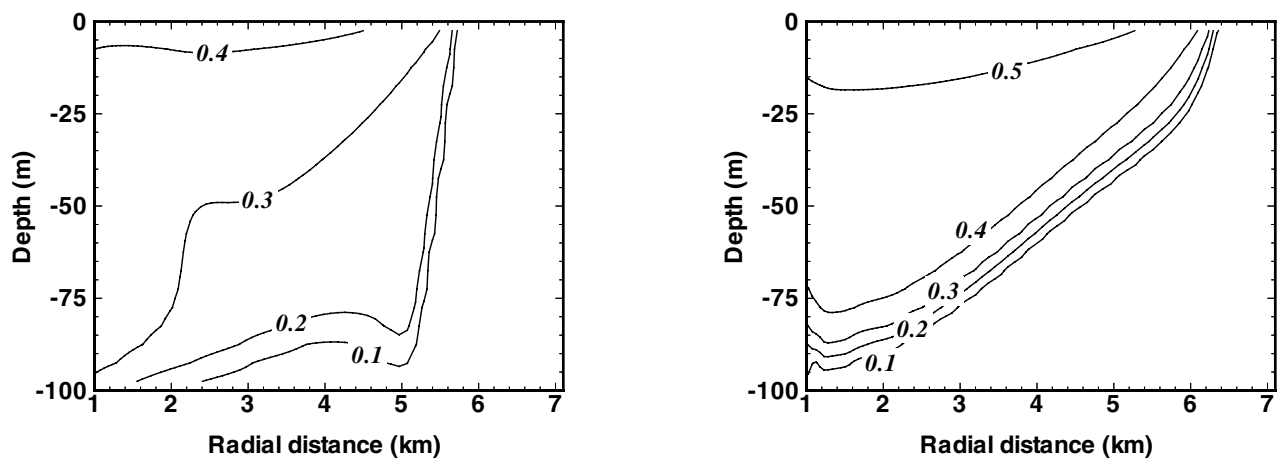

(a) (b)

Figure 6. Simulated gas saturations after 30 years for the two anisotropic cases, with ratios of horizontal to vertical permeability of 10:1 (a) and 1:1 (b). Depth is measured relative to the top of the aquifer.

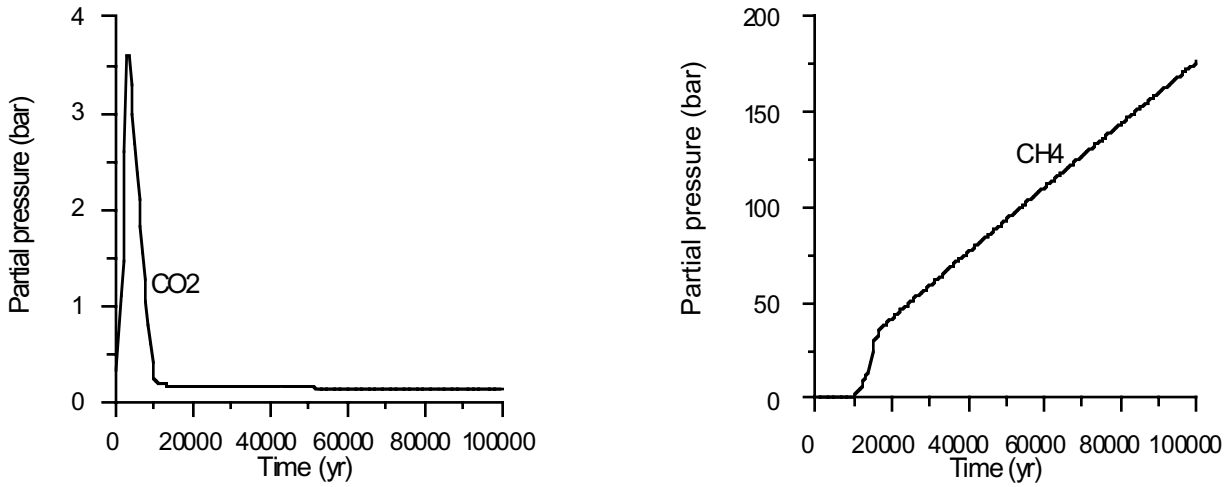

(a) (b)

Figure 7. Distribution of gas partial pressures obtained for the glauconitic sandstone case (without CO2 injection).

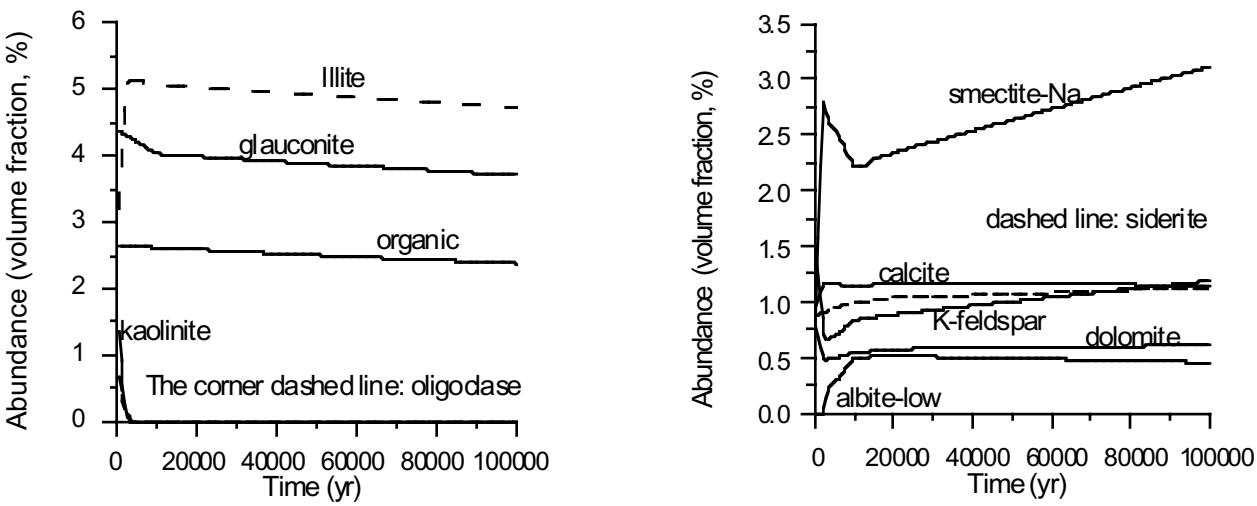

(a) (b)

Figure 8. Distribution of mineral abundances for the glauconitic sandstone case (without CO2 injection).

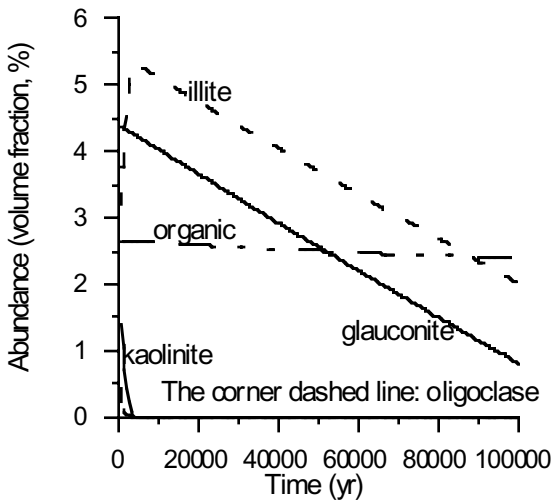

(a)

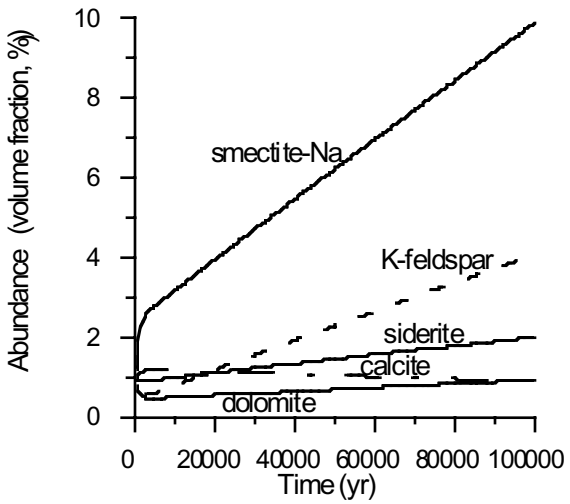

(b)

Figure 9. Distribution of mineral abundances in glauconitic sandstone (with CO2 injected at 260 bar).

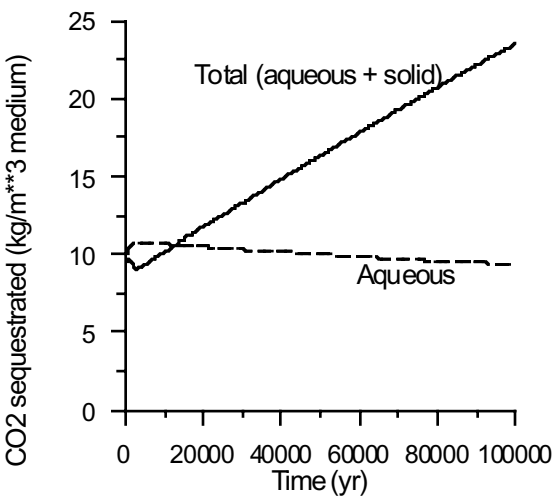

Figure 10. Cumulative CO2 sequestration in glauconitic sandstone (with CO2 injected at 260 bar).

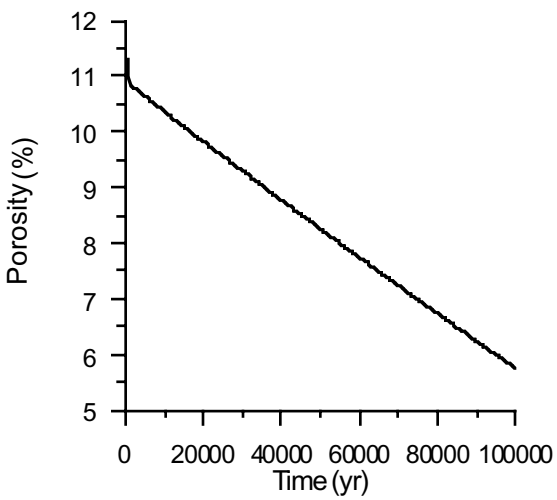

Figure 11. Porosity evolution in glauconitic sandstone (with CO2 injected at 260 bar).